Flapping Flight for Biomimetic Robotic Insects Part II: Flight Control Design

Xinyan Deng, Luca Schenato, and Shankar Sastry,
Department of Electrical Engineering and Computer Sciences
University of California at Berkeley
{*xinyan,lusche,sastry*}*@eecs.berkeley.edu*

***Abstract*— In this paper we present the design of flight control algorithms for flapping wing micromechanical flying insects (MFIs). Inspired by the sensory feedback and neuromotor structure of biological flying insects, we propose a similar top-down hierarchical architecture to achieve high performance despite the MFIs' limited computational resources. Flight stabilization is formulated as high frequency periodic control of an underactuated system. In particular, we provide a methodology to approximate the time-varying body dynamics caused by the aerodynamic forces with time-invariant dynamics using averaging theory and a biomimetic parametrization of wing trajectories. This approximation leads to a simpler dynamical model that can be identified using experimental data from the onboard sensors and the input voltages to the wing actuators. Moreover, the overall control law is a simple periodic proportional output feedback. Simulations, including sensor and actuator models, demonstrate stable flight in hovering mode.**

***Index Terms*— flapping flight, micro aerial vehicles, biomimetic, periodic control, averaging.**

I. Introduction

The recent interest in micro aerial vehicles (MAVs) [1], largely motivated by the need for aerial reconnaissance robots inside buildings and confined spaces, has galvanized the development of inch-size flapping wing MAVs that could mimic at least part of the extraordinary performance of insect flight. This is a challenging endeavor for several reasons. First, aerodynamics for inch-size flapping robots differ greatly from manmade fixed or rotary-winged vehicles [2]. Second, size constraints forbid the use of rotary electric motors and commercial inertial navigation system (INS), global positioning systems (GPS) and current cameras. Finally, a flapping frequency beyond $100Hz$ requires sensors and processing algorithms with bandwidth and sensitivity at least one order of magnitude higher than those usually found in today's aircrafts. Nonetheless, recent technological advances, together with better understanding of insect aerodynamics and biomechanics have promoted projects aimed at the design of Micromechanical Flying Insects (MFIs) [3] [4].

The goal of this paper is to develop a general framework to design a control unit for MFIs which would enable them to accomplish complex autonomous tasks such as searching, surveillance and monitoring. This paper builds upon a companion paper [5] where comprehensive modeling of MFI aerodynamics, body dynamics, sensors, and electromechanical actuation is presented together with a list of references to relevant research. Here, we focus on the control aspects of flapping flight for MFIs. In particular, we propose a hierarchical architecture for the control unit that mimics the sensory feedback and neuromotor structure of biological flying insects to achieve high performance while satisfying MFIs physical and computational constraints. One of the major contributions of this paper is to approximate the time-varying (TV) dynamics of insect flight caused by the flapping wings with a simpler time-invariant (TI) system whose controllers can then be formulated using standard control design tools. This approximation relies on two ideas that can be formalized within the framework of high-frequency control theory. The first key idea is that the frequency of the aerodynamic forces acting on the insect is much larger than the bandwidth of body dynamics, and, therefore, only the mean aerodynamic forces and torques affect the insect dynamics. The second idea is to parameterize the wing trajectory within a wingbeat period using some biologically inspired wing kinematic parameters, which affect the distribution of aerodynamic forces within the wingbeat, thus modulating the total forces and torques acting in the insect center of mass. These parameters appear as virtual inputs in the TI approximation of flight dynamics. Finally, we show how the parameters of the TI approximation can be identified directly from sensors measurements and actuators input voltages obtained from experiments from the true TV system. This approach is particularly suitable for flapping flight since it does not require the knowledge of exact aerodynamics models, which are particularly complex. Also, it provides a model for uncertainty caused by sensor and actuator nonlinearities and external disturbances that can be used to design robust controllers.

The paper is organized as follows. In Section II, we briefly review biological literature about insect flight control mechanisms, focusing on the interaction between the sensory system and the neuromotor architecture. In Section III the hierarchical architecture of flight control observed in true insects, and the helicopter attitude-based navigation are then used as a model for the design of an equivalent control system for MFIs. In Section IV we highlight analogies and differences between flapping flight and helicopter flight. In Section V we propose a formal approach to approximate the time-varying insect dynamics with a time invariant dynamics based on averaging theory and wing trajectory parametrization. Section VI presents the design of the input voltage to the actuators that is required to track a desired wing trajectory. In Section VII we model insect dynamics as a discrete time dynamical system where the input are the kinematic parameters

This work was funded by ONR MURI N00014-98-1-0671,ONR DURIP N00014-99-1-0720 and DARPA.

Authors are with the Robotics and Intelligent Machines Lab in the Department of Electrical Engineering and Computer Sciences at the University of California at Berkeley

defined in the previous section. Closed-loop identification is then implemented to estimate the discrete-time system. The identified model is then used to design LQR-based feedback laws for hovering. Finally, in Section VIII, conclusions and future research directions are presented.

II. Insect Flight Sensors and Control Mechanisms

Flies have inhabited our planet for over 300 million years, and today they account for more than 125,000 different species, so that, by now, roughly every tenth known species is a fly [6]. This evolutionary success might spring from their insuperable maneuverability and agility to survive, which enable them, for example, to chase mates at turning velocities of more than $3000^o s^{-1}$ with delay times of less than 30 ms.

The extraordinary maneuverability exhibited by flying insects is the result of a sophisticated neuromotor control system combined with highly specialized sensors. These sensors comprise of the pressure sensilla, the halteres, the ocelli, and the compound eyes.

Pressure force sensilla are present along the wing surface, the wing base, the halteres, and other parts of the body. Although their functionality in flight control is not clear, they might play an important role in estimating the instantaneous air flow around the wing and in controlling the wing trajectory.

The *halteres*, two oscillating club-shape appendices, are the biological equivalence of a gyroscope, and they are used to estimate the body angular velocity.

The *ocelli*, a sensor system composed of three wide-angle photoreceptors oriented in a tetrahedron configuration, can estimate insect orientation relative to the horizon by comparing the light intensity from different regions of the sky.

The *compound eyes* serve the purpose of estimating large-field optical flow, small-field object fixation, and object recognition. The large-field optical flow estimated from the compound eyes can provide information about the orientation, the angular velocity, and the linear velocity which can guarantee excellent performance when combined with ocelli and halteres [7]. The large-field optical flow from the compound eyes, together with ocelli and halteres, play the role of the inertial navigation system (INS) in insect flight. Furthermore, compound eyes can also perform specialized visual processing for object fixation and landmark recognition, which is used to navigate the environment and estimate proximity of obstacles and targets.

A more detailed description for these sensors from a flight control perspective can be found in [7] [5] and in the references therein.

At present, still little is known about the flight control mechanisms and neuromotor physiology in true insects [8] [9] [6]. Experimental evidence suggests the existence of at least two levels of control, as shown in Fig. 1. At the lower level the halteres and the ocelli control the wings muscles directly in order to keep stable flight orientation. This level of control seems to be reactive, since it mediates corrective reflexes to compensate for external disturbances and to maintain a stable flight posture. At the high level, the brain, stimulated by visual and physiological stimuli, plays the role of a navigation planner, which plans a trajectory based on its ultimate goal, such as foraging or chasing a mate. Differently from the

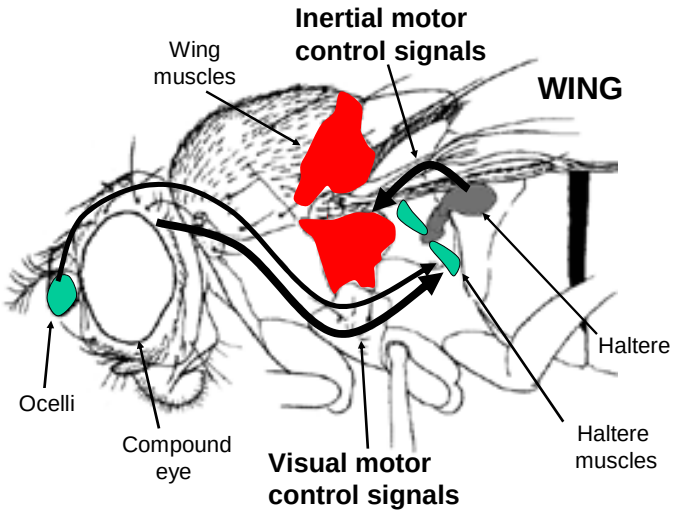

Fig. 1. Neuromotor control physiology in flying insect.

halteres-ocelli system, the visual system is not connected directly to the wing muscles, but to the halteres muscles. Therefore, this level of control indirectly affects the flight behavior by biasing the motion of the halteres, thus creating an apparent external disturbance that the lower level of control would try to compensate for. This structure is similar to that between the vestibular-ocular reflexes and active head rotation in vertebrates [10]. The reason for this hierarchical control architecture is probably an efficient solution to resolve the conflict between flight stability reflexes and goal-orientated manoeuvres. This typical biological neuromotor control architecture is shown in the left side of Fig. 2. Without some appropriate inhibiting mechanism, the haltere-mediated equilibrium reflexes would always counter goal-oriented motions. To resolve this potential conflict, the nervous system must contain the means of attenuating equilibrium reflexes during the generation of controlled maneuvers.

Another sublevel, as part of the reactive control system, might be present and associated with the pressure sensors which innervate the wings and the haltere. This bottom level might adjust wing motion within a single wingbeat to improve aerodynamic efficiency and compensate for local turbulence [11].

The hierarchical structure of neuromotor control in true insects has been adopted as a guiding model for the design of the control unit for MFIs, as described in the next section.

III. Hierarchical Control Architecture

The hierarchical architecture, partially inspired by true flying insects and autonomous aerial robots research [12], decomposes the original flight control problem into a set of hierarchical modules, each responsible for a specific task. This way, the controllers in each module can be designed independently of those on higher levels, thus allowing the possibility to incrementally build more and more articulated control structures. Fig. 2 shows the architecture proposed for the MFI control unit. It is possible to identify three main levels: the *navigation planner*, the *flight mode stabilizer* and the *wing trajectory controller*. The top level is a voluntary one since planning is determined by MFI goal, the two lower levels are more reactive since the purpose of the flight mode stabilizers

and the wing kinematic generator is to maintain the desired flight posture and the desired wing trajectory in the presence of external disturbances, respectively. Each of these three levels in the control unit receive specific sensory information from different sensors.

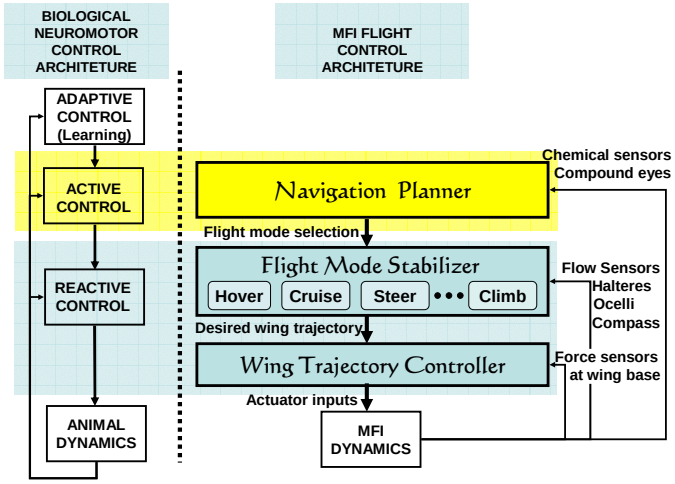

Fig. 2. Design architecture for the control unit of the MFI compared to the neuromotor control architecture present in most animals.

At the top level of the control unit there is the *navigation planner*. Besides sensory input from the visual system, this unit can receive commands from a communication link and information from application-specific sensors such as chemical or temperature sensors. The purpose of this module is to choose a sequence of appropriate flight modes for the flight mode stabilizer level, which enables the MFI to safely navigate the environment and achieve the desired task such as territory exploration, target localization and tracking.

The middle level is the *flight mode stabilizer* which is responsible for stabilizing different flight modes available to the MFI, such as take off, hovering, cruising, steer left, steer right, climb, dive, and land. Each flight mode is achieved by a dedicated controller that uses as inputs the signals from the halteres, the ocelli, the large-field optical flow estimates, and a magnetic compass. Based on this information, the controller chooses the appropriate values for the desired torques and forces that must be applied to MFI body to compensate possible disturbances and to maintain the desired flight mode. The desired torques and forces are then mapped directly into the corresponding wing trajectory for the next wingbeat, as shown in Section V-C.

The bottom level is the *wing trajectory controller* which is responsible for generating the electrical signals for the actuators in order to track the desired wing motion generated by the flight mode stabilizer module. The set of possible wing trajectories is parameterized according to some biokinematic parameters, as described in Section V-C. These parameters are chosen based on biomimetic principles, i.e. by changing them it is possible to replicate most of the wing trajectories observed in true insects. The most important biokinematic parameters are the stroke angle amplitude and offset, timing of rotation, mean angle of attack, and upstroke-to-downstroke wing speed ratio. The active change of these parameters by true insects have been observed to be directly correlated to specific maneuvers and flight modes [13]. Then every wing trajectory is mapped to the corresponding actuator voltages via another map, as described in Section VI. The wing trajectory controller receives input information from force sensors placed at the wing's base. This sensory information can be directly used to estimate instantaneously the position and velocity of the wing, thus improving wing motion control through feedback.

IV. Insect versus Helicopter Flight

Similar to aerial vehicles that are based on rotary wings, such as helicopters, flying insects control their flight by controlling their attitude and the magnitude of the vertical thrust [13]. Position and velocity control is achieved via attitude control, in fact forces acting on a plane parallel to the ground can be generated by tilting and banking the body. Pitching down, for example, would result in a forward thrust, while rolling sideward would result in a lateral acceleration. Altitude control is achieved via mean lift modulation, for example, by increasing the vertical force would result in an upward acceleration and vice versa.

However, there are some peculiar differences that prevent one from directly applying successful flight control techniques developed for helicopters [14]. The spinning of the rotor blade induces a reaction yaw torque on the helicopter body that would make the latter rotate in the opposite direction if not compensated by the tail rotor. On the other hand, the tail rotor generates a lateral thrust that needs to be compensated by tilting the helicopter body sideways. This problem is not present in insect flight since the wings oscillate almost symmetrically on the opposite side of the insect body, therefore inertial forces cancel out. Another very important difference is the intrinsic time varying nature of the aerodynamics in insect flight. As shown in Fig. 5 the aerodynamic forces and torques generated by the wings change dramatically during a wingbeat, and cannot be assumed to be constant as in the case of the helicopter. One additional difference is that the wing trajectory cannot change dramatically from one wingbeat to the next, since the wings need to oscillate to generate sufficient lift to sustain the insect weight. Finally, in insect flight the two wings can follow asymmetric trajectories. This peculiar characteristic allows insects to generate large angular accelerations by modulating the distribution of the aerodynamic forces within a wingbeat, without strongly affecting the mean lift generation. The dependence between wing motion and torque generation in true insects has recently been considered in [15].

These similarities and differences lead us to consider the following strategy when designing a robust stabilizing hovering controller. First, we will model the insect dynamics as a Discrete Time Linear Time Invariant (DTLTI) system based on the average forces and torques over a wingbeat. This approach is based on high frequency control theory that guarantees good approximation error between the original time-varying system and averaged system, assuming that the wingbeat frequency is sufficiently high [16]. Moreover, the design for the controller is based on a MFI dynamics model obtained through an identification procedure that includes the approximation errors due to the time varying nature of the dynamics.

Second, we parameterize the wing kinematics with four parameters, such that they can be mapped uniquely into the three mean torques (roll, pitch, yaw) and mean lift. This approach

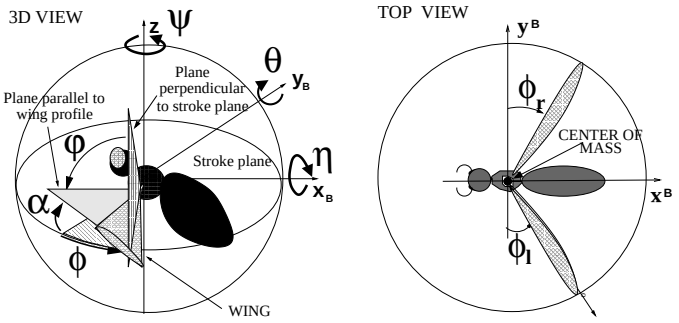

Fig. 3. Definition of wing kinematic parameters: (*left*) 3D view of insect body and left wing, (*right*) top view of insect stroke plane.

allows a direct control of the torques and lift generation, thus simplifying the control design for the attitude and altitude of the MFI. The dynamics of the insect is then linearized about the hovering equilibrium point and we propose some approximations that decompose the original MIMO system into four SISO subsystems. Finally, the controller is based on robust state feedback based on linear-quadratic regulator (LQR) design.

V. High Frequency Insect flight control

A. Insect dynamics

As shown in [5], the insect dynamics can be written as:

$$\begin{aligned} \ddot{\Theta} &= (\mathcal{I}W)^{-1}[\tau_a^b(t) - W\dot{\Theta} \times \mathcal{I}W\dot{\Theta} - \mathcal{I}\dot{W}\dot{\Theta}] \\ \ddot{\mathbf{p}} &= -\frac{c}{m}\dot{\mathbf{p}} - \mathbf{g} + \frac{1}{m}Rf_a^b(t) \end{aligned} \quad (1)$$

where $\tau_a^b \in \mathbb{R}^3$ and $f_a^b \in \mathbb{R}^3$ are the torque and force vectors generated by wing aerodynamics relative to the insect center of mass. The vector $\Theta = [\eta\ \theta\ \psi]^T$ represents the ZYX Euler's angles (roll,pitch,yaw), $W = W(\Theta)$ is the transformation matrix from body angular velocity, ω^b, to Euler's angular velocity, $\dot{\Theta}$, i.e. $\dot{\Theta} = W\omega^b$. $\mathcal{I}$ is the insect moment of inertia relative to the body frame, $\mathbf{p}$ is the position of the insect center of mass relative to the fixed frame, $\mathbf{g} = [0\ 0\ -g]^T$ is the gravity vector, c is the linear damping coefficient, and $R = e^{\hat{z}\psi}e^{\hat{y}\theta}e^{\hat{x}\varphi}$ is the rotation matrix. This notation is commonly found in spacecraft and helicopter dynamics textbooks such as [17] and [14]. The wrench, i.e. the forces and torques, due to the aerodynamic forces is a nonlinear function of the position and velocity of the wing stroke angle, ϕ, and the angle of attack, α, of both wings, i.e.

$$\begin{aligned} f_a^b(t) &= f_a^b(\phi_r, \phi_l, \varphi_r, \varphi_l, \dot{\phi}_r, \dot{\phi}_l, \dot{\varphi}_r, \dot{\varphi}_l) = f_a^b(u, \dot{u}) \\ \tau_a^b(t) &= \tau_a^b(\phi_r, \phi_l, \varphi_r, \varphi_l, \dot{\phi}_r, \dot{\phi}_l, \dot{\varphi}_r, \dot{\varphi}_l) = \tau_a^b(u, \dot{u}) \end{aligned} \quad (2)$$

where $u = (\phi_r, \phi_l, \varphi_r, \varphi_l)$, and the lowerscripts r, l stand for right and left wing, respectively. The stroke angle is the angle between the wing radial axis and the y-axis of the stroke plane. The rotation angle is defined as the angle between the vertical plane and the wing profile, which corresponds to the complement of the angle of attack α, i.e. $\alpha = 90^o - |\varphi|$ (see Fig. 3). The explicit expression of aerodynamics forces and torques as a function of wing kinematics can be found in [5]. The aerodynamic forces and torque are the only time-varying element in Equations (1), otherwise the insect dynamics would be very similar to the time-invariant nonlinear dynamics of a helicopter. On the other hand, the wingbeat period is much smaller than the responsiveness of the insect body, therefore, intuitively speaking, only mean forces and torques are relevant. In fact, this approximation has been formalized by averaging theory [16], and high-frequency periodic control has been successfully applied to trajectory tracking and approximate stabilization of underactuated systems [18] [19] [20]. However, few tools are available to synthesize the control laws systematically and they are mainly limited to mechanical systems with specific geometric properties [21] [22]. In particular, these tools derive a suitable time-varying input parametrization $u = g(v,t)$ directly from the structure of the flow of the dynamics, $\dot{x} = f(x,u) = f_0(x) + F(x)u$. In our case, we do not directly apply these tools because of the complexity of the aerodynamic forces and torques, and thus of the vector flow, as function of the wing's angles and velocity u. One possible approach to designing the control laws is the adoption of a linearized model of insect aerodynamics and apply the aforementioned tools, however this approach is likely to give poor results in practice, since insect aerodynamics is a highly nonlinear function of wing position and velocity. Instead, we propose to parameterize the wing motion based on biomimetic principles to design our periodic inputs, i.e. we propose $u = g(v,t)$. Then, by applying averaging theory to approximate the complex time varying dynamics with the average time invariant dynamics, we show that there is a direct map between the proposed kinematic parameters and the mean forces and torques. The kinematics parameters appear as virtual inputs in the averaged dynamics. The averaged dynamics is then suitable to standard controller design similarly to those found in helicopter control.

B. Averaging

Averaging theory and high frequency control encompass several results and they have been applied in different scientific areas. Recently, these results have been applied specifically to insect flight [23]. Here we report only some of the results that we will use for the flight controller design.

Theorem 1 ([23]). *Let us consider the following systems:*

$$\begin{cases} \dot{x} &= f(x,u,\dot{u}) \\ u &= g(v,t) \\ v &= h(x) \\ g(v,t) &= g(v,t+T) \end{cases} \quad (3)$$

$$\begin{cases} \dot{\bar{x}} &= \bar{f}(\bar{x},v) \\ \bar{f}(x,v) &= \frac{1}{T}\int_0^T f(x,g(v,t),\dot{g}(v,t))dt \\ v &= h(\bar{x}) \end{cases} \quad (4)$$

where $x, \bar{x} \in \mathbb{R}^n, u \in \mathbb{R}^m, v \in \mathbb{R}^p$, and all functions and their partial derivatives are continuous up to second order.

If $\bar{x} = 0$ is an exponentially stable equilibrium point for the averaged system (4), then $x(t) - \bar{x}(t) = O(T)$ for all $t \in [0,\infty)$. Moreover the original system (3) has a unique, exponentially stable, T-periodic orbit $x_T(t)$ with the property $||x_T(t)|| < kT$.

In our setting, T is the wingbeat period, and the system $f(x,u)$ is given by Equations (1) and (2), where the vector $u = (\phi_r, \phi_l, \varphi_r, \varphi_l)$ represents the right and left wing angles. As it will be shown in the next section, the wing trajectories

are chosen to be T-periodic functions and are parameterized by a parameter vector v, i.e. $u = g(t, v)$. The parameter vector v can be interpreted as a vector of virtual inputs. Therefore, as indicated by the theorem, rather than trying to analyze the original system we will focus on its averaged dynamics given by Equations (1) where the time-varying wrench $(f_a^b(t), \tau_a^b(t))$ given in Equations 2 is substituted with its average:

$$\begin{aligned} \bar{f}_a^b(v) &\triangleq \frac{1}{T}\int_0^T f_a^b(g(t,v), \dot{g}(t,v))dt \\ \bar{\tau}_a^b(v) &\triangleq \frac{1}{T}\int_0^T \tau_a^b(g(t,v), \dot{g}(t,v))dt \end{aligned} \quad (5)$$

which is time-independent and depends only on the virtual input vector v. We will then look for exponentially stabilizing control feedback law $v = h(x)$ for the averaged systems. If such a function exists, then the original time-varying system will have a bounded error from the desired equilibrium point if the wingbeat period T is sufficiently small. Although this approach does not guarantee asymptotic stability for the original system, we will show that the error bound kT is very small for insect flight as observed in true insects, and therefore irrelevant from a practical point of view.

C. Wing Kinematic Parametrization

Although it is currently unclear how true insects accomplish the control of their flight and maneuvering capabilities, recent work has found that by modulating a few kinematic parameters on each wing, such as wing rotation timing at the stroke reversals and the wing blade angle of attack, the insect can readily apply torques on the body and, therefore, control its attitude and position [2] [13]. Based on this observation, it was suggested that a small set of wing kinematics might be sufficient to generate all possible flight modes, and the key point for designing any of these modes is the capability to control the MFI's attitude [24].

In particular, the research done by Dickinson and his group [2] has suggested that the following kinematic parameters may suffice to generate any flight maneuver: *timing of rotation*, *mean angle of attack*, *stroke angle amplitude* and *stroke angle offset*. There is a strong evidence that if these parameters can be controlled independently, then it is possible to control the torque and force generation during flapping. For example, a large (small) stroke angle amplitude would generate a large (small) lift. An advanced (delayed) timing of rotation at the end of the downstroke results in a nose-up (nose-down) pitch torque. A larger (smaller) angle of attack during the downstroke relative to the upstroke produces a backward (forward) thrust. Most true insects flap their wings along a symmetric trajectory with a stroke angle amplitude around 120^o and mean angle of attack of 45^o on both downstroke and upstroke [25] [6]. However, during saccades and other maneuvers, they modify the wing trajectory by changing the kinematic parameters described above [26].

Based on these biologically inspired arguments, the problem to solve then is how to parameterize the wing trajectory to be able to mimic the real insects by *independently* controlling the biokinematic parameters described above. We will then show how the parameters map directly to the mean torques and forces, thus simplifying the design of a flight stabilizer. More specifically, the wing trajectory during a wingbeat is

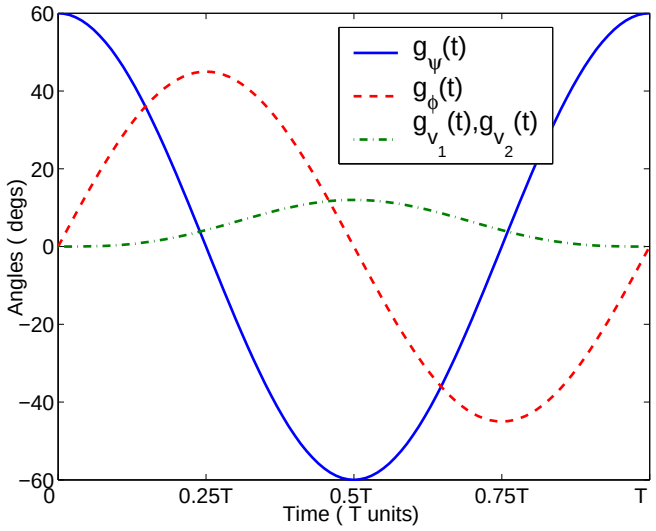

Fig. 4. Wing kinematic parameterizing functions given in Equations (8).

described using the stroke angle, ϕ and the rotation angle φ. In particular, we parameterize the wing motion of each wing within a wingbeat period as follows:

$$\phi(t; v) = g_\phi(t) + v_1\, g_1(t) \quad (6)$$
$$\varphi(t; v) = g_\varphi(t) + v_2\, g_2(t) \quad (7)$$

where the functions $g_i(t)$ are T-periodic function, i.e. $g_i(t + T) = g_i(t)$, (v_1, v_2) are the kinematic parameters, and T is the wingbeat period. These functions are chosen based on the considerations above. In particular, $g_\varphi(t)$ and $g_\phi(t)$ generate a symmetric motion with maximum lift production, $g_1(t)$ modifies only the stroke angle amplitude, $g_2(t)$ modifies the timing of rotation of the angle of attack at the end of the downstroke. Based on observations of true insect flight we choose the following functions:

$$\begin{aligned} g_\phi(t) &= \frac{\pi}{3}\cos(\frac{2\pi}{T}t) \\ g_\varphi(t) &= \frac{\pi}{4}\sin(\frac{2\pi}{T}t) \\ g_1(t) &= \frac{\pi}{15}\sin^3(\frac{\pi}{T}t) \\ g_2(t) &= g_1(t) \end{aligned} \quad (8)$$

which are defined on the interval $t \in [0, T)$ and extended by periodicity so that $g_i(t + T) = g_i(t)$. Fig. 4 shows a pictorial representation of wing motion and corresponding aerodynamic forces for different choices of the kinematic parameter v_1 and v_2. Note how these parameters affect the distribution of forces along the whole wingbeat period.

The wing parametrization given by Equations (8) is not unique and might not be optimal either, however it gives rise to wing trajectories that mimic some of the trajectories observed in true insects. In fact, a positive (negative) value for v_1 results in a large (small) stroke angle amplitude; a positive (negative) value for β results in a delayed (advanced) timing of rotation at the end of the downstroke. If this parametrization above is replicated for both wings, the wings kinematics $u = (\phi_r, \phi_l, \varphi_r, \varphi_l)$ can be written in terms of the parameters

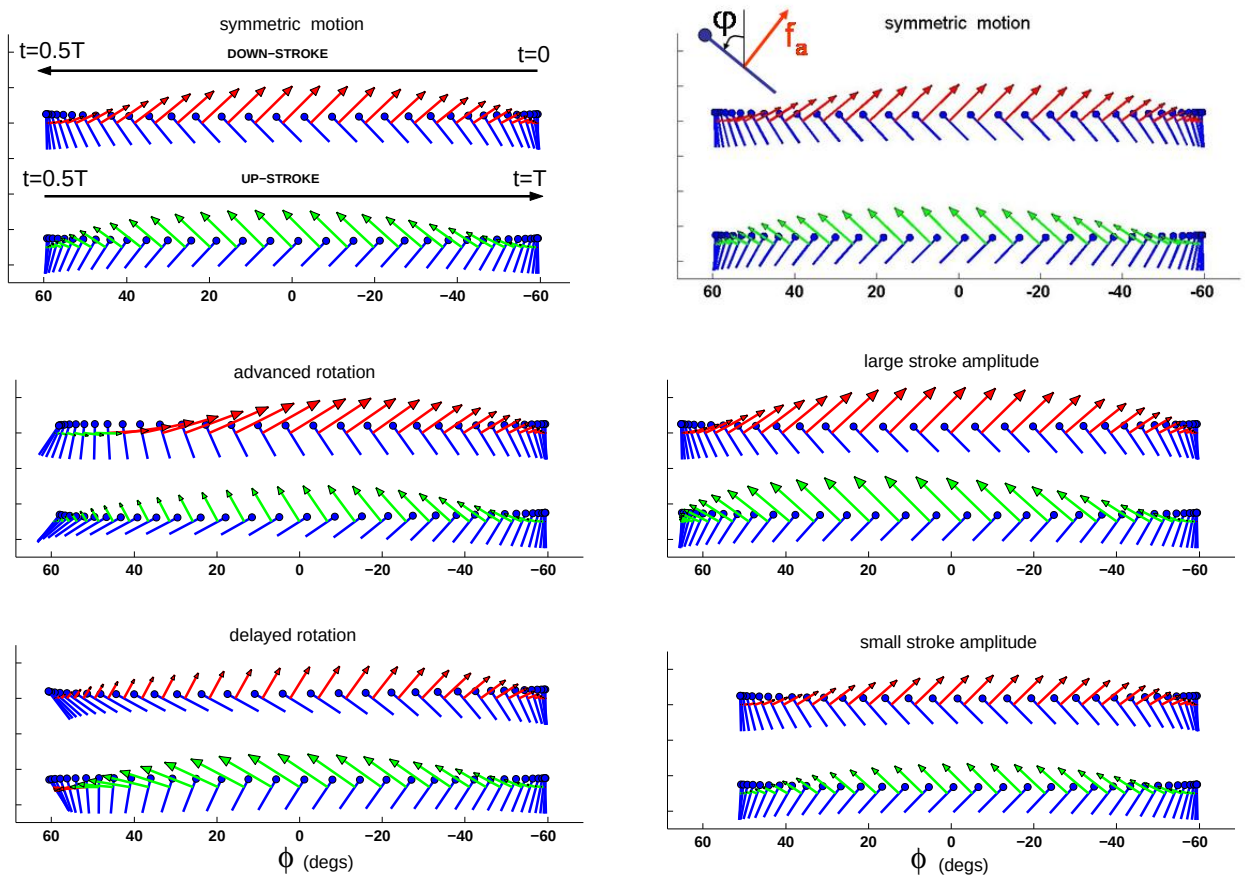

Fig. 5. Pictorial sequence of the side view of wing motions and the corresponding aerodynamic forces for different choice of kinematic parameters. Symmetric motion: $v_1 = 0, v_2 = 0$. Advanced rotation: $v_1 = 0, v_2 = 1$. Delayed rotation: $v_1 = 0, v_2 = -1$. Large stroke amplitude: $v_1 = 1, v_2 = 0$. Small stroke amplitude: $v_1 = -1, v_2 = 0$.

$v = (v_1^r, v_1^l, v_2^r, v_2^l)$ as follows:

$$u(v,t) = g(t) + G(t)v \tag{9}$$
$$g = \begin{bmatrix} g_\phi \\ g_\phi \\ g_\varphi \\ g_\varphi \end{bmatrix}, G = \begin{bmatrix} g_1 & 0 & 0 & 0 \\ 0 & g_1 & 0 & 0 \\ 0 & 0 & g_2 & 0 \\ 0 & 0 & 0 & g_2 \end{bmatrix}$$

where $g(t)$ and $G(t)$ are a T-periodic vector and matrix, respectively, whose entries are defined in Equations (8).

It is now possible to study the effect of the chosen parametrization on the mean wrench. In fact, if we substitute Equation (9) into Equations (5), we obtain a static map $\Pi : \mathbb{R}^4 \to \mathbb{R}^6$ from the wings parameters $v \in \mathbb{R}^4$ to the mean wrench $(\bar{f}_a^b, \bar{\tau}_a^b) \in \mathbb{R}^6$:

$$\begin{bmatrix} \bar{f}_a^b \\ \bar{\tau}_a^b \end{bmatrix} = \Pi(v) \tag{10}$$

This is a nonlinear map and cannot be computed analytically since the aerodynamic force and torque are complex functions of wing position and velocity (see Section IV in [5]). However, one could look for an affine approximation around the origin of the wings parameters:

$$\begin{bmatrix} \bar{f}_a^b \\ \bar{\tau}_a^b \end{bmatrix} = \pi_0 + \Pi_l v + \delta(v) \tag{11}$$

where $\pi_0 \in \mathbb{R}^6$, $\Pi_l \in \mathbb{R}^{6\times 4}$, and $\delta(v)$ is the approximation error. Although, it is not possible to linearize analytically Equation (11) to obtain π_0 and Π_l directly, it is possible to randomly select different values for the parameter vector v, substitute it into the parametrization given by Equation (9), and finally compute the true mean wrench $(\bar{f}_a^b, \bar{\tau}_a^b)$ via simulations using the exact wing aerodynamics. The approximating π_0 and Π_l can then be found by rewriting Equation (11) as a least square (LS) problem where (π_0, Π_l) are the unknowns. Simulations are performed based on the aerodynamic model described in [5], and on the morphological body parameter of a typical blowfly, which is the MFI target model. The approximating affine map is found to be as follows:

$$\pi_0 = \begin{bmatrix} 0 \\ 0 \\ mg \\ 0 \\ 0 \\ 0 \end{bmatrix}, \Pi_l = 0.1mg \begin{bmatrix} 0 & 0 & -1.0 & -1.0 \\ 0 & 0 & 0.3 & -0.3 \\ 0.9 & 0.9 & 0 & 0 \\ 0.4L & -0.4L & -0.1L & 0.1L \\ -0.2L & -0.2L & -0.4L & -0.4L \\ 0 & 0 & -0.5L & 0.5L \end{bmatrix} \tag{12}$$

where m is the mass of the insect, L is the length of the wing, and the zero entries correspond to estimated values negligible relative to the largest entries in the matrix. This approximation is quite accurate for kinematic parameters smaller than unity, $||v||_\infty \leq 1$. Fig. 6 shows that the estimated mean wrench, $w = \pi_0 + \Pi_l v$, predicts quite accurately the true mean wrench

obtained from simulations, thus validating our approach.

The particular structure of this map is a consequence of the parameterization based on the biological insights described at the beginning of this section. In fact, as we expect, any component of the wrench depends additively or differentially on two parameters, depending if the wings are moving symmetrically or anti-symmetrically. Note that along the z-component the symmetrical wing motions generate a vertical lift sufficient to balance insect body weight. The magnitude of the coefficients in the map are considerable. In fact, the insect can generate forward or vertical thrust in the order of $\bar{f}_a \approx 0.1{-}0.2\,mg$, and angular torques of order $\bar{\tau}_a = 0.1 - 0.2\,mLg$. In other words, considering that the moment of inertia of a true insect along one of its principal axis is on the order of $I \approx 0.1mL^2$ [25] and that our target size wing is $L = 10\text{mm}$, this is equivalent to saying that the insect can generate linear accelerations of about $a_{lin} = \bar{f}_a/m = 0.2g \approx 2\,\text{m/s}^2$ and angular accelerations of about $a_{ang} = \bar{\tau}_a/I = g/L \approx 10^5 \text{deg/s}^2$, which are comparable with those observed in true insects.

Inspecting the structure of this parameters-to-wrench map, it is apparent that the three mean torques and the vertical thrust can be controlled almost independently by appropriately choosing the values for the four wing parameters v. However, there are small but non-negligible couplings between some of the wrench components. For example, a positive (negative) pitch torque is always associated to a positive (negative) forward thrust. Similarly, a positive (negative) yaw torque is associate with a small positive (negative) roll torque and a small negative (positive) lateral force. Although this is undesirable, it does not undermine the stabilizability of flight modes, as we will show in the next section. Besides, this coupling is not particularly harmful. In fact, as in helicopters, forward motion in MFIs is obtained by pitching down the body orientation. Since a pitch down torque generation is associated with a positive forward thrust generation, the coupling actually improves responsiveness rather than reducing it.

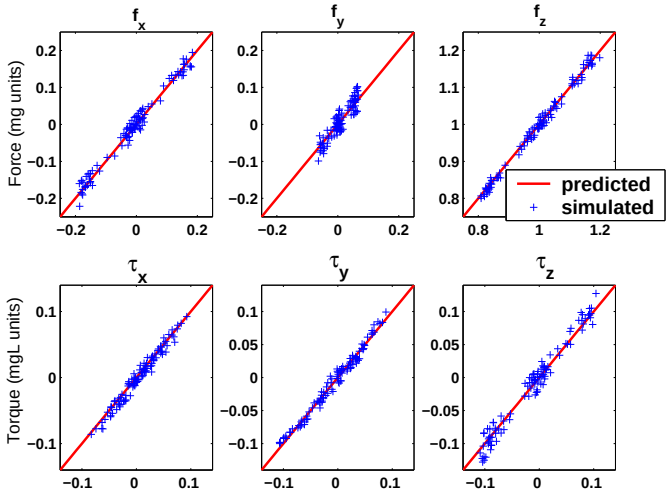

Fig. 6. Predicted mean wrench $w = \pi_0 + \Pi_l v$ (x-axis) versus the exact mean wrench (y-axis) obtained from simulations for 100 random values of the wings parameter vector v in the unit box, i.e. $||v||_\infty \leq 1$. The spreading around diagonal lines quantifies the modeling errors.

We can summarize this section by saying that, although it is not possible to control instantaneously the insect wrench, there exist wing motions that can control independently the *mean* forces along the z-axis and the torques about all three axes. We also showed that the affine parameterization of wing motions given by Equations (9), based on biomimetic principles, gives rise to a simple affine map between the mean wrench and the kinematic parameters. Based on the averaging arguments exposed in the previous section, where the input u and the parameter vector or virtual input v as defined in Theorem 1, correspond to the wing angles $u = (\phi_r, \phi_l, \varphi_r, \varphi_l)$ and kinematic parameters $v = (v_1^r, v_1^l, v_2^r, v_2^l)$. Also, based on the fact that the three mean torque components and the vertical thrust can be controlled independently, it is clear that this is a sufficient condition to design stabilizing controllers for insect flight. In the next section, we will show how to design stabilizing controllers for the linearized averaged dynamics that also stabilize the original nonlinear time-varying dynamics.

VI. Wing Trajectory Tracking and Actuator Control

The previous section described how to design wing trajectories that can generate the desired mean forces and torque during a wingbeat period. However, the wing trajectory cannot be controlled directly, and appropriate input voltages to the thorax actuators must be devised to track the desired wing trajectory. As described in [5], the dynamics of the thorax-wing structure can be approximated as a stable 2-degree of freedom second order system. Given a desired wing trajectory $(\phi_d(t), \varphi_d(t))$, we can calculate the corresponding steady-state input voltages by substitution:

$$\begin{bmatrix} V_{1,d}(t) \\ V_{2,d}(t) \end{bmatrix} = T_0^{-1}\left(M_0 \begin{bmatrix} \ddot{\phi}_d(t) \\ \ddot{\varphi}_d(t) \end{bmatrix} + B_0 \begin{bmatrix} \dot{\phi}_d(t) \\ \dot{\varphi}_d(t) \end{bmatrix} + K_0 \begin{bmatrix} \phi_d(t) \\ \varphi_d(t) \end{bmatrix} \right) \tag{13}$$

where $T_0, M_0, B_0, K_0 \in \mathbb{R}^{2\times 2}$ are constant matrices, and V_1, V_2 are the input voltages to the wing actuators. Let $V = (V_1^l, V_1^r, V_2^l, V_2^r)$ be the input voltages for the two wings, and $u = (\phi_r, \phi_l, \varphi_r, \varphi_l)$, then the wing-thorax dynamics for both wings can be rewritten as follows:

$$M\ddot{u} + B\dot{u} + Ku = V \tag{14}$$

where M, B, K are matrices that depend on T_0, M_0, B_0, K_0, and the dynamics is stable. As we will show in the next Section, the flight mode stabilizer is assumed to be able to select a new wing trajectory at the beginning of every wingbeat among those defined by the parametrization in Equations (7) and (8). This is equivalent to saying that given any sequence $\{v_n\}_{n=0}^{\infty}$, where $v = (v_1^r, v_1^l, v_2^r, v_2^l)$ is the wing kinematics parameter vector as defined in the previous section, the wing trajectory controller must track the trajectory:

$$u_d(t) = g(t) + G(t)v(t), \tag{15}$$

$$v(t) = v_n, \qquad t \in [nT, (n+1)T) \tag{16}$$

where $g(t)$ and $G(t)$ are defined in Equation (9). Note that the matrix $G(t)$ defined in Equations (8) was specifically chosen to have the additional property

$$G(0) = \dot{G}(0) = \ddot{G}(0) = G(T) = \dot{G}(T) = \ddot{G}(T) = 0 \tag{17}$$

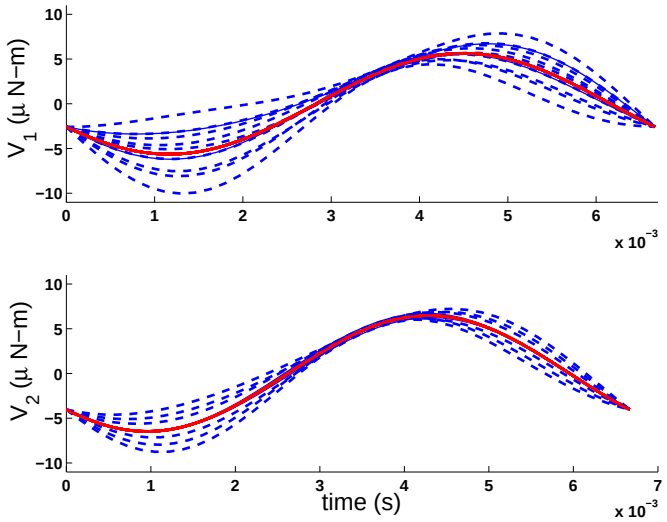

Fig. 7. Actuator voltage profile as defined in Equation (18) for 10 random values of parameter vector v with $||v||_\infty \leq 1$. The solid line corresponds to $v = 0$, i.e. $V_d(t) = h(t)$. Note that $||V_d(t)||_\infty \leq 10\mu$N for all $||v||_\infty \leq 1$.

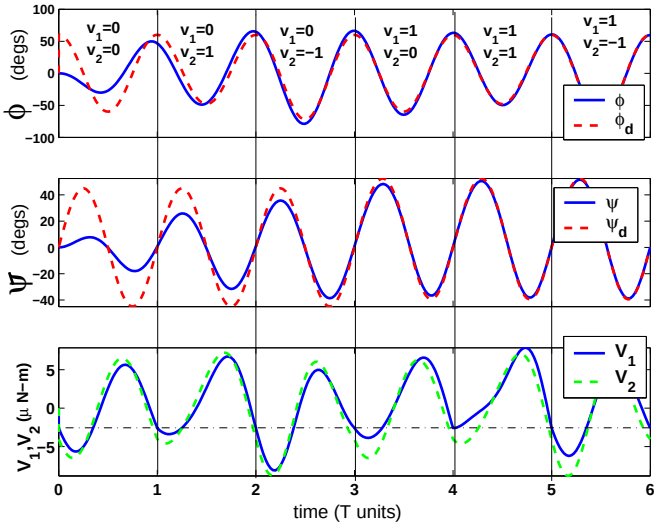

Fig. 8. Simulation of actuator control given in Equations (18) showing asymptotically tracking of desired trajectory for a random sequence of kinematic parameters $\{v_n\}$, where $v = (v_1, v_2)$, and random initial condition of actuator state vector, for one wing. From bottom to top: actuator voltages V_1, V_2 as given by Equation (18) (*bottom*). Rotation angle, φ, (*center*), and stroke angle, ϕ, (*top*), given by Equation (14). The error between desired and true wing trajectory decays after approximately 3 wingbeat periods.

and, therefore, the trajectory $u_d(t) \in \mathcal{C}^2$ is continuous up to its second derivative for any sequence $\{v_n\}$. If we substitute Equation (15) into Equation (14) we formally obtain:

$$\begin{aligned} V_d(t) &= h(t) + H(t)v(t) && (18)\\ v(t) &= v_n, \qquad t \in [nT, (n+1)T) && (19)\\ h(t) &= M\ddot{g}(t) + B\dot{g}(t) + Kg(t) \\ H(t) &= M\ddot{G}(t) + B\dot{G}(t) + KG(t) \end{aligned}$$

where $h(t)$ and $H(t)$ are a T-periodic vector and matrix, respectively. Since $H(t)$ is simply a linear combination of $G(t)$ and its first and second derivatives, then it follows from Equation (17) that $H(0) = H(T) = 0$. This implies that the input voltage vector $V_d(t) \in \mathcal{C}^0$ is continuous for any sequence $\{v_n\}$.

Let us consider a desired wing trajectory vector $u_d(t)$ defined by Equations (9) and the corresponding feasible input voltage vector $V_d(t)$ defined by Equations (18). We define the wing trajectory tracking error to be $e_u = u - u_d$, and apply input voltage $V_d(t)$, then we have:

$$\begin{aligned} M\ddot{e}_u &= -B\dot{e}_u - Ke_u \\ \dot{e}_u(0) &= \dot{u}(0) - \dot{u}_d(0), \quad e_u(0) = u(0) - u_d(0) \end{aligned}$$

where we used Equation (14) and the fact $\ddot{u}_d(t) = -B\dot{u}_d(t) - Ku_d(t) + V_d(t)$ for all $t \in [0, \infty)$. Since the system above is stable, we have that $\lim_{t\to\infty} e_u(t) = 0$, or equivalently $\lim_{t\to\infty} u(t) = u_d(t)$ for any initial condition. The rate of decay, $1/\tau_{decay}$, is set by the poles of the wing-thorax mechanical system. The time constant τ_{decay} is approximately 1 to 2 wingbeat periods for the target MFI design. This property guarantees that even if we cannot directly control the wing trajectory, any initial perturbation would disappear within a few wingbeats and the wing trajectory would converge exponentially to the steady-state solution, as shown in Fig. 8.

The wing trajectory tracking approach developed in this section is equivalent to a feed-forward control of wing trajectory during a single wingbeat. In fact, it allows trajectory changes only at the beginning of every wingbeat in such as way that this transition is smooth and there is no error between desired wing trajectory an actual wing trajectory. This is equivalent to saying that there is no error between the desired and actual mean wrench during the following wingbeat. This approach has two main advantages. The first advantage is that we can assume to have direct control of the wing trajectory, and we can neglect the wing-thorax dynamics since any perturbation would die off within a few wingbeats. The second advantage is that it naturally leads to a discrete time (DT) system, since the wing kinematic parameters v are updated every T seconds, i.e. at the beginning of every wingbeat. We will exploit these two properties in the next Section by modelling the insect dynamics as a discrete time system where the inputs are the wing kinematic parameters v and the state is the mean value of the body linear and angular position and velocity within the previous wingbeat.

VII. Flight Control in Hover

Following the guidelines described in the previous section, we can now look for a stabilizing controller for hovering by designing a feedback law $v = h(x)$ such that the origin of the averaged system is exponentially stable.

A. Identification

The analysis in the previous section provides a torque decoupling scheme together with a set of virtual control inputs, i.e. the wing kinematic parameters v, which enters into the averaged system in a affine fashion. Since we are interested in the insect dynamics close to the hovering regime where angular deviations and angular velocities are small,

we linearize the averaged system dynamics near hover. We approximate the continuous-time nonlinear system, with a DTLTI model in the following form:

$$\begin{array}{rcl} x(n+1) & = & Ax(n) + Bv(n) + \delta(n) \\ y(n) & = & x(n) + \eta(n) \end{array} \quad (20)$$

where $x = [\bar{\eta}_x \ \bar{\theta}_y \ \bar{\psi}_z \ \bar{\omega}_x \ \bar{\omega}_y \ \bar{\omega}_z \ \bar{p}_x \ \bar{p}_y \ \bar{p}_z \ \bar{v}_x \ \bar{v}_y \ \bar{v}_z]^T$ is the vector of average roll, pitch, and yaw angles, angular velocities, positions and linear velocities over one wingbeat, respectively; $\delta(n)$ represents the unmodelled dynamics as well as external disturbances which appear as an external noise to the linear model. This term includes both process noise as well as unmodeled non-linearities. The input vector $v = [v_1^r \ v_1^l \ v_2^r \ v_2^l]^T$ are the wing kinematic parameters, which appear as virtual control inputs. The measurement vector $y = [\bar{y}_2^o \ \bar{y}_1^o \ \bar{y}^c \ \bar{y}_1^h \ \bar{y}_2^h \ \bar{y}_3^h; \bar{y}_1^e \ \bar{y}_2^e \ \bar{y}_3^e \ \bar{y}_4^e \ \bar{y}_5^e \ \bar{y}_6^e]^T$ is the vector of measured outputs from the ocelli, halteres, magnetic compass, and compound eyes, with additional measurement noise $\eta(n)$. As described in [5], these measurements correspond to an estimate of the insect true state, i.e. $y = \hat{x}$.

The matrices $[A, B]$ can be obtained analytically from MFI morphological parameters such as mass, moment of inertia, center of mass, etc. However, these parameters are difficult to obtain in practice. Moreover, this approach cannot model the effect of the time varying part of the aerodynamic forces. Another approach would be to substitute the parameter-to-wrench map into the original nonlinear dynamics and linearize it. Here we adopted the system identification approach, *i.e.*, run a large number of experiments and record the pair $[y(n), v(n)]$ of sensor measurements and kinematic parameters, and then find the matrices $[A, B]$ that best fit the data. Moreover, further investigation into the particular structure of the insect dynamics given in Equation (20) results in the following approximate linear system to be identified:

$$A = \begin{bmatrix} I_{3\times3} & TI_{3\times3} & 0_{3\times3} & 0_{3\times3} \\ 0_{3\times3} & A_{22} & 0_{3\times3} & 0_{3\times3} \\ 0_{3\times3} & 0_{3\times3} & I_{3\times3} & TI_{3\times3} \\ A_{41} & 0_{3\times3} & 0_{3\times3} & A_{44} \end{bmatrix}, \ B = \begin{bmatrix} 0_{3\times3} \\ B_{21} \\ 0_{3\times3} \\ B_{41} \end{bmatrix}$$

where T is the wingbeat period, the matrices A_{22} and A_{44} account for angular and linear damping, and the matrix A_{41} accounts for the linear accelerations due to tilted body orientation. This structure is typically used in helicopter dynamics identification [27] [28].

We first estimate a model in open loop where only data for the first several wingbeats are recorded. Since the sensor measurements provide an estimate for all the entries of the state vector, the model identification problem can be recast into a least square solution to an overdetermined set of linear equations as $Ez = d$, where $z = [a_{i,j}, ..., b_{k,h}]^T$ is the vector of system parameters to be estimated, and $a_{i,j}$ and $b_{k,h}$ are the nonzero entries of the matrices A and B respectively. The matrix $E = E(y(\cdot), u(\cdot))$ and $d = d(y(\cdot))$ are matrices whose entries depend on the experimental data. The least square solution which minimizes the norm of the error $||e||^2 = ||d - Az||^2$ is given by $z = E(E^TE)^{-1}E^Td$. The experiments were performed on the Virtual Insect Flight Simulator (VIFS), developed by the authors to provide a software testbed for insect flight [5]. The experimental data were generated with random inputs and initial conditions near the hovering equilibrium.

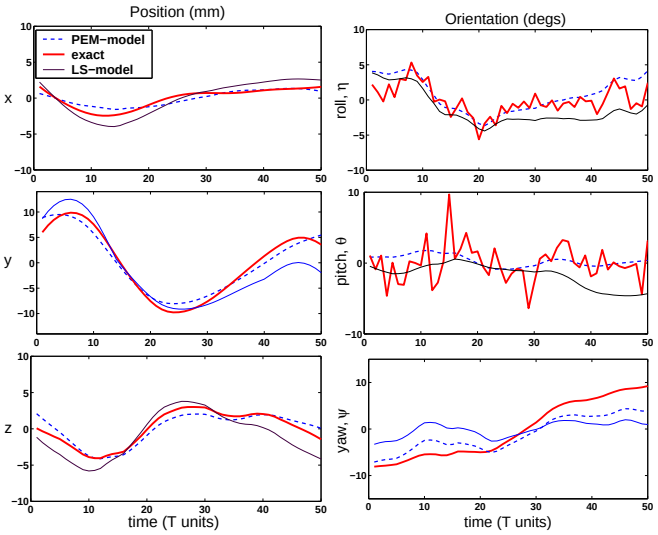

Fig. 9. Comparison of the exact mean angles and angular velocities (*thick solid line*) with those predicted with the PEM-based DTLTI model (*dashed line*), the LS-based DTLTI model (*thin solid line*) and those simulated using exact model over 50 consecutive wingbeats.

Based on this least-squared-based model $[A, B]$, a stabilizing state feedback control based on pole placement was designed and tuned first on the nominal LTI model, then verified on the fully nonlinear continuous time dynamics provided by VIFS. Although least-squared identification is simple and straightforward, it does not exploit the structure of the dynamics present in Equation (20), nor does it provide a systematic way to estimate process and output noise. However, it does provide a stabilizing controller which can be used successively to perform closed loop system identification through prediction error method (PEM) [29]. The prediction error method cannot be applied directly to the system (20), since the system is unstable, which is why least-square identification is performed first. The PEM-based identified model performed better than the least-squared-based one in predicting insect dynamics as shown in Fig. 9. Besides, the estimated process and noise variances and biases can be used to design better robust controllers.

B. Controller design

In order to address the trade off between regulation performance and control effort to avoid control input saturation, and also to take into account process disturbances and measurement noise in Equation (20), we employed a Linear Quadratic Gaussian (LQG) optimal controller design.

As a first step, a state feedback LQR regulator $v = -Kx$ was designed to minimize the following quadratic cost function

$$J = \lim_{N\to\infty} E(\sum_{n=1}^{N} x(n)^T Q x(n) + v(n)^T R v(n)) \quad (21)$$

where $Q \geq 0$ and $R > 0$ are the weighting matrices that define the trade-off between regulation performance and control effort. The controller was designed with standard discrete-time LQG software, and the diagonal entries in the weighting

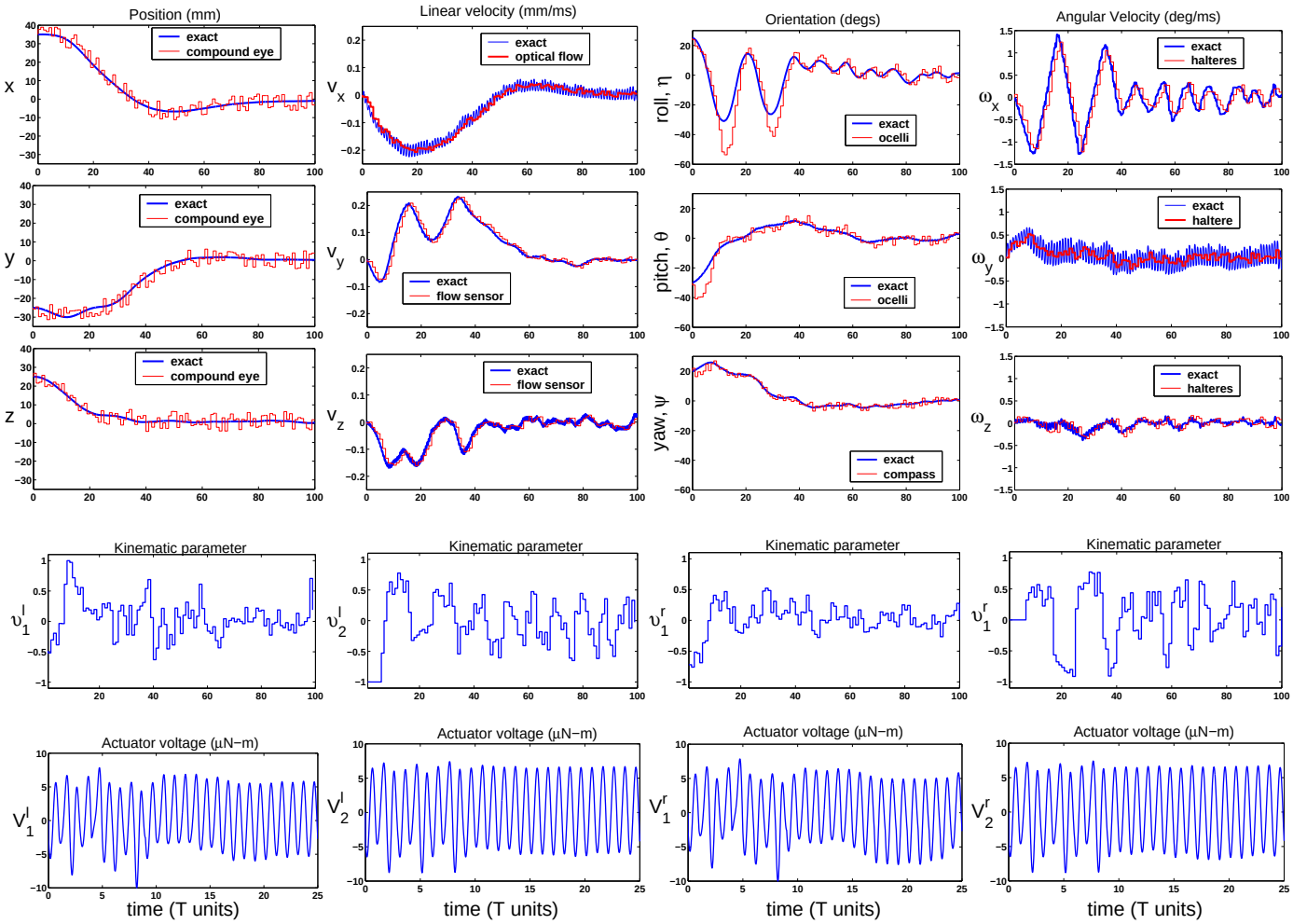

Fig. 10. Simulation of hovering control with sensor feedback and actuators dynamics. From top to bottom: insect true state and sensors measurements (*row 1-3*); kinematics parameters given by Equation (22) (*row 4*); actuators voltage given by Equation (23)(*row 5*) during the first 25 wingbeats.

matrices are iteratively tuned to ensure a good transient response without saturating the control inputs. The above LQR optimal state feedback $v = -Kx$ is then substituted with a more realistic output feedback:

$$v(n) = -Ky(n), \tag{22}$$

where the output y is given by the sensors measurements. As described earlier, the simplified DTLTI system (20) provides a feedback scheme to select the wing kinematic parameter for the next wingbeat period. The true feedback control from sensor measurements to actuator voltages is obtained by combining Equation (22) with Equation (18) to give:

$$\begin{aligned} V_d(t) &= h(t) + H(t)v(t) = h(t) + H(t)Ky(t) \\ &= h(t) + \tilde{K}(t)y(t) \qquad (23) \\ y(t) &= y(nT), \qquad t \in [nT, (n+1)T) \qquad (24) \end{aligned}$$

where the sensors measurements are sampled at the beginning of each wingbeat, and $\tilde{K}(t)$ is simply a proportional T-periodic matrix gain. It is remarkable that a simple proportional T-periodic feedback scheme is sufficient to stabilize the complex time-varying nonlinear insect dynamics including nonlinear sensor measurements, actuator dynamics, and process and output noise. More importantly, this gain can be computed off-line and easily stored on the computation unit of the MFI.

The LQR controller was finally tested on the fully nonlinear time-varying model which includes the MFI dynamics of Equation (1), the wing-thorax dynamics of Equations (13), and the sensor models described in [5]. The simulations are based on a target MFI of $100mg$ and $10mm$-wingspan with wingbeat frequency $f = 150Hz$. Fig. 10 shows a simulation for hovering stabilization from the initial condition $x = (\eta_x, \theta, \psi, \omega_x, \omega_y, \omega_z, p_x, p_y, p_z, v_x, v_y, v_z) = (25^o, -25^o, 20^o, 0, 0, 0, 35mm, -25mm, 25mm, 0, 0, 0)$, and wing state $(u, \dot{u}) = (\phi_r, \phi_l, \varphi_r, \varphi_l, \dot{\phi}_r, \dot{\phi}_l, \dot{\varphi}_r, \dot{\varphi}_l) = 0$. Our proposed controller design successfully achieved stabilization despite sensor and process noise. The initial condition corresponds to an offset from the desired position of about 3 body-lengths. The steady state error during hovering is $< 1/10$ of the body-length for the position and $< 5^o$ for the orientation. The MFI requires about 50 wingbeat periods T to reach the

final configuration, which corresponds to about $2/3$rds of a second for a wingbeat frequency of $150Hz$.

C. Single channel identification and control design

Based on the particular structure of the mean wrench map given in Equation (12), where it appears that the mean torque and the vertical thrust can be controlled almost independently by combining symmetrically or anti-symmetrically the kinematic parameters $v = (v_1^r, v_1^l, v_2^r, v_2^l)$, we can reformulate the flight control problem of the 6 DOF system similar to that of helicopter control, where we have decoupled the system dynamics into longitudinal, lateral, heave, and yaw dynamics [14] [28]. In fact, if we redefine the kinematic parameters as follows:

$$\tilde{v} = (\tilde{v}_1, \tilde{v}_2, \tilde{v}_3, \tilde{v}_4) = (v_1^r - v_1^l, v_2^r + v_2^l, v_2^r - v_2^l, v_1^r + v_1^l) = Fv \quad (25)$$

and we use these parameters as inputs for the system (20) and repeat the identification process, then we obtain the following matrices:

$$\begin{aligned} A_{41} &= \begin{bmatrix} 0 & a_4 & 0 \\ -a_4 & 0 & 0 \\ 0 & 0 & 0 \end{bmatrix}, & A_{22} &= \text{diag}\{a_1, a_2, a_3\}, \\ & & A_{44} &= 0_{3\times 3}, \\ B_{21} &= \begin{bmatrix} b_1 & 0 & * & 0 \\ 0 & b_2 & 0 & * \\ 0 & 0 & b_3 & 0 \end{bmatrix}, & B_{41} &= \begin{bmatrix} 0 & * & 0 & 0 \\ 0 & 0 & * & 0 \\ 0 & 0 & 0 & b_4 \end{bmatrix} \end{aligned} \quad (26)$$

where the zeros entries are entries that were much smaller than the other entries in the same row, and the asterisks, $*$'s, indicate non-negligible entries. If the $*$'s are neglected, it is clear that each virtual parameter $\tilde{v}_i$ controls independently one of the three angular accelerations and the vertical acceleration, thus justifying the single channel controller design scheme as typically done for a helicopter. The advantage of this approach is that the feedback matrix gain is given by:

$$K_{\tilde{v}} = \text{diag}\{K_{long}, K_{lat}, K_{heav}, K_{yaw}\} \quad (27)$$

where the matrices $K_{long}, K_{lat}, K_{heav}, K_{yaw}$ are the smaller size proportional gain matrices obtained from the decoupled insect flight dynamics, thus reducing the computational burden when computing the feedback $\tilde{v} = K_{\tilde{v}} y$. Fig. 11 shows a comparison between the full channel controller design and the single channel design. The performance using single channel design degrades somewhat, but it is less computationally demanding than the full channel design, which is a clear advantage for the limited computational unit available to MFIs.

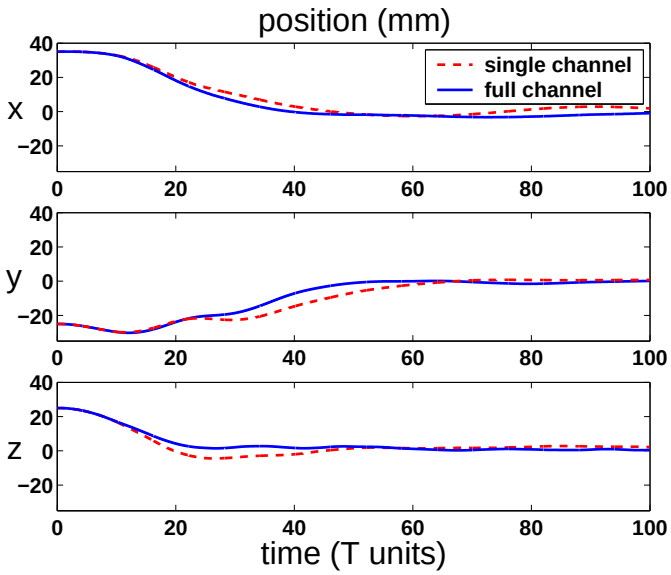

Fig. 11. Comparison of single channel design vs full channel design.

VIII. Conclusion

In this paper we presented an framework for flapping flight control and navigation in biomimetic robotic insects. We started by reviewing the neuromotor architecture present in true flying insects, and highlighting analogies and differences between insect flapping flight and helicopter flight. Inspired by true insect neuromotor organization of flight control mechanisms, we proposed a three-layered hierarchical control structure that simplify flight control design while preserving the high maneuverability and the agile navigation capability exhibited by true insects. The first major contribution of this paper was to propose a suitable parametrization of wing motion during the course of a full wingbeat and to combine it with averaging theory arguments, thus showing that the insect time-varying dynamics can be well approximated by a discrete-time linear time-invariant (DTLTI) system where the wing kinematic parameters appear as virtual inputs. The second major contribution was to propose an identification-based LQR controller design which does not required the knowledge of an accurate model for the insect morphological parameters, such as moment of inertia and mechanical part's sizes, nor an accurate model of the aerodynamics. As a result, hovering flight mode can be stabilized with a simple affine T-periodic proportional feedback from sensor measurements to actuator voltages. This is very important considering the limited computational resources available to MFI's. Although in this paper we focused on hovering, it has been shown that other flight modes like cruising and steering can be stabilized using a affine T-periodic proportional feedback [30].

Several research directions can be explored. The most important one is probably in regard to the wing parametrization, which in this paper was based on the observations of true insect wing motions. However, different wing kinematic parameters could be chosen. Therefore, a more systematic methodology to optimize the wing trajectory parametrization with respect to some metrics, such as aerodynamic power or maximum torque production, is sought.

Another direction emerges from wing trajectory tracking. One of the major assumptions in our approach was the linearity of the actuator dynamics, so that wing trajectory tracking could be easily solved using a pseudo-inverse to compute the control input to the actuators. This assumption is true only to the first order, as shown in [31], and nonlinearities become particularly important when rapid wing rotations at the end of the half-strokes are necessary for aggressive flight maneuvers. Novel approaches need to be considered in this scenario.

Finally, navigation and searching algorithms in unknown environments have not been explored in this paper and it is part of our current research.

REFERENCES

[1] B. Motazed, D. Vos, and M. Drela, "Aerodynamics and flight control design for hovering MAVs," in *Proceedings of American Control Conference*, Philadelphia, PA, June 1998, pp. 681–683.

[2] M.H. Dickinson, F.-O Lehmann, and S.S. Sane, "Wing rotation and the aerodynamic basis of insect flight," *Science*, vol. 284, no. 5422, pp. 1954–1960, 1999.

[3] R.S. Fearing, K.H. Chiang, M.H. Dickinson, D.L. Pick, M. Sitti, and J. Yan, "Wing transmission for a micromechanical flying insect," in *Proceeding of IEEE International Conference on Robotics and Automation*, 2000, pp. 1509–1516.

[4] R.C. Michelson and M.A. Naqvi, "Beyond biologically inspired insect flight," in *von Karman Institute for Fluid Dynamics RTO/AVT Lecture Series on Low Reynolds Number Aerodynamics on Aircraft Including Applications in Emergening UAV Technology*, Brussels, Belgium, 2003, pp. 1–19.

[5] X. Deng, L. Schenato, W.C. Wu, and S.S. Sastry, "Flapping flight for biomimetic robotic insects. Part I: System modeling," *Submitted to IEEE Transactions on Robotics*.

[6] R. Dudley, *The Biomechanics of Insect Flight: Form, Function, Evolution*, Princeton: University Press, 2000.

[7] L. Schenato, W.C. Wu, and S.S. Sastry, "Attitude control for a micromechanical flying insect via sensor output feedback," *IEEE Transactions on Robotics and Automation*, vol. 20, pp. 93–106, April 2004.

[8] W.P. Chan, F. Prete, and M.H. Dickinson, "Visual input to the efferent control system of a fly's "gyroscope"," *Science*, vol. 280, no. 5361, pp. 289–292, 1998.

[9] A. Fayyazuddin and M.H. Dickinson, "Haltere afferents provide direct, electrotonic input to a steering motor neuron of the blowfly," *Journal of Neuroscience*, vol. 16, no. 16, pp. 5225–5232, 1996.

[10] G. Sandini, F. Panerai, and F.A. Miles, "The role of inertial and visual mechanisms in the stabilization of gaze in natural and artificial systems," *Motion Vision - Computational, Neural, and Ecological Constraints*, pp. 189–218, 2001.

[11] R. Hengstenberg, "Mechanosensory control of compensatory head roll during flight in the blowfly *Calliphora erythrocephala*," *Journal of Comparative Physiology A-Sensory Neural & Behavioral Physiology*, vol. 163, pp. 151–165, 1988.

[12] H.J. Kim, D.H. Shim, and S.Sastry, "A flight control system for aerial robots: Algorithms and experiments," *Control Engineering Practice*, vol. 11, no. 12, pp. 1389–1400, 2003.

[13] G.K. Taylor, "Mechanics and aerodynamics of insect flight control," *Biological Review*, vol. 76, no. 4, pp. 449–471, 2001.

[14] R.W. Prouty, *Helicopter Performance, Stability, and Control*, Krieger Publishing Company, 1995.

[15] S.P. Sane and M.H. Dickinson, "The control of flight force by a flapping wing: Lift and drag production," *Journal of Experimental Biology*, vol. 204, no. 15, pp. 2607–2626, 2001.

[16] J.A. Sanders and F. Verhulst, *Averaging methods in Nonlinear Dynamical Systems*, Springer-Verlag, New York, N.Y., 1985.

[17] B. Wie, *Space vehicle dynamics and control*, AIAA Educational Series, Reston, VA, 1998.

[18] N.E. Leonard, "Periodic forcing, dynamics and control of underactuated spacecraft and underwater vehicles," in *Proceedings of 34th IEEE Conference on Decision and Control*, New York, USA, 1995, pp. 3980–3985.

[19] K.A. Morgansen, V. Duindam, R.J. Mason, J.W. Burdick, and R.M. Murray, "Nonlinear control methods for planar carangiform robot fish locomotion," in *Proceedings of the IEEE International Conference on Robotics and Automation*, Seoul, South Korea, May 2001, pp. 427–434.

[20] J. Ostrowski and J.W. Burdick, "The mechanics and control of undulatory locomotion," *International Journal of Robotics Research*, vol. 17, no. 7, pp. 683–701, 1998.

[21] P.A. Vela, *Averaging and Control of Nonlinear systems (with application to Biomimetic Locomotion)*, Ph.D. thesis, California Institute of Technology, 2003.

[22] S. Martínez, J. Cortés, and F. Bullo, "On analysis and design of oscillatory control systems," *IEEE Transactions on Automatic Control*, vol. 48, no. 7, pp. 1164–1177, 2003.

[23] L. Schenato, *Analysis and Control of Flapping Flight:from Biological to Robotic Insects*, Ph.D. thesis, University of California at Berkeley, December 2003.

[24] L. Schenato, X. Deng, and S.S. Sastry, "Flight control system for a micromechanical flying insect: Architecture and implementation," in *Proceeding of IEEE International Conference on Robotics and Automation*, 2001, pp. 1641–1646.

[25] C.P. Ellington, "The aerodynamics of hovering insect flight. I-VI," *Philosophical Transactions of the Royal Society of London B Biological Sciences*, vol. 305, pp. 1–181, 1984.

[26] S.N. Fry, R. Sayaman, and M. H. Dickinson, "The aerodynamics of free-flight maneuvers in *Drosophila*," *Science*, vol. 300, no. 5618, pp. 495–498, April 2003.

[27] J.C. Morris, M. Nieuwstadt, and P. Bendotti, "Identification and control of a model helicopter in hover," in *Proceedings of the American Control Conference*, Baltimore, Maryland, 1994, vol. 2, pp. 1238–1242.

[28] D. H. Shim, H. J. Kim, and S. Sastry, "System identification and control synthesis for rotorcraft-based unmanned aerial vehicles," in *Proc. of the IEEE International Conference on Control Applications*, Anchorage, September 2000, pp. 808–813.

[29] L.J. Ljung and E.J. Ljung, *System Identification: Theory for the User*, Prentice Hall, 1998.

[30] X. Deng, L. Schenato, and S. Sastry, "Attitude control for a micromechanical flying insect including thorax and sensor models," in *Proc. of the IEEE International Conference on Robotics and Automation*, Taipei, Taiwan, May 2003, pp. 1152–1157.

[31] S. Avadhanula, R.J. Wood, D. Campolo, and R.S. Fearing, "Dynamically tuned design of the MFI thorax," in *Proc. of the IEEE International Conference on Robotics and Automation*, Washington, DC, May 2002, pp. 52–59.